

Numeric Investigation of Non-Stationary Dust-Containing Airflow and Deposition of Dust Particles with Various Sizes in the Lower Airways

Trusov P.V.^{1,2}, Zaitseva N.V.¹, Tsinker M.Yu.^{*1,2}, Kuchukov A.I.^{1,2}

¹*Federal Scientific Center for Medical and Preventive Health Risk Management Technologies, Perm, Russia*

²*Perm National Research Polytechnic University, Perm, Russia*

Abstract. Within creation of the mathematical model to describe the human respiratory system, we accomplished numeric investigation of non-stationary dust-containing airflow as well as dust particle deposition in the lower airways with the real anatomic geometry based on CT scans. Inhaled air is considered a multi-phase mixture of a homogenous gas and solid dust particles. Motion of a basic carrier gas phase is described using the Euler approach (the viscous flow model). Solid dust particles are a dispersed carried phase, which is described with the Lagrange approach. The $k-\omega$ model is used to describe turbulence. We consider non-stationary airflow during calm inhalation. The article presents calculated flow streamlines for the velocity of particles in inhaled air in the lower airways at different moments. We quantified a share of deposited particles (SDP) with various dispersed structure (between 10 nm and 100 μm) and density (1000 kg/m^3 , 2000 kg/m^3 , 2700 kg/m^3) in the lower airways; the article provides computed motion paths of particulate matter. Solid particle deposition in the airways has different efficiency depending on particle sizes and density. SDP goes down as their sizes and masses decrease. Particle density mostly influences differences in deposition of micro-sized particles (2.5–20 μm): as particle mass and density grow, a share of particles deposited in the airways also increases. SDP for particles with their diameter being less than 1 μm amounts to approximately 20 % of all the particles that reach the entry to the trachea. According to the results obtained by numeric modeling, the greatest share of dust particles penetrates the right main bronchus, predominantly the right middle and inferior lobar bronchi. Dust particles are able to induce diseases of the lungs, pneumoconiosis included.

Key words: *human airways, numeric modeling, non-stationary process, dust particles, micro- and nano-sized particles, share of deposited particles, particle density*

INTRODUCTION

Many research works provide evidence of harmful effects produced on human health by ambient air pollution with chemicals [1–3] and dust emissions from industrial facilities [4–7]. Particulate matter in ambient air, depending on its chemical and dispersed structure, is able to produce multiple adverse effects on health, respiratory diseases included [8, 9]. Metals and organic compounds can often be found on the surface of particulate matter; they enhance negative effects on human health.

*cinker@fcrisk.ru

We have been developing a mathematical model of the human respiratory system to quantify inhalation introduction of harmful chemicals and dust particles into the human body, as well as to predict diseases caused by environmental exposures [10]. In this model, the respiratory system is described by a set of sub-models: the sub-model of the transition zone (upper [11] and lower airways [12]), where air moves from the atmosphere to the lungs and back, and the submodel of the respiratory zone (the lung segments with alveoli where gas exchange takes place) [13].

Since methods and means of computational gas dynamics for investigating processes occurring in the human respiratory system have been developing quite intensively, more and more attention is now paid to three-dimensional models describing airflow as a multi-component gas mixture moving inside channels with complex shapes [14–28].

Reconstructing the geometry of the modeling area (shapes of the airways) is a specific sub-task within investigating airflow in the airways. Previously, studies relied on a simplified geometry of the lower respiratory tracts that used simple geometric shapes (cylindrical tubes with round cross-sections of various diameters); they were based on morphological data about sizes (diameters and lengths) and angles of the airways [14–18, 10, 12]. Thus, the authors of the study [15, 17, 18] used a symmetric geometry of the lower airways based on data provided by E.R. Weibel [29]; a non-symmetric geometry was used in [14, 16, 10; 12].

Up-to-date mathematical models developed in this area tend to be personalized and to consider an actual three-dimensional geometry of the airways based on CT scans [20–28].

Airflow in the airways is investigated based on reconstructed three-dimensional shapes under different respiration conditions. The existing studies mostly examine airflow and dust particle deposition under stationary respiration (usually, they consider flow rates at the entry (Q_{in}) equal to 15 L/min, 30 L/min, and 60 L/min) [22–25]. Estimations of particles deposition differ significantly under different respiration conditions (preset boundary conditions) and disperse structures of particles. Thus, the study [22] focused on investigating stationary flow of dusty air and particle deposition in the section of the airways from the mouth to bronchioles. There, it was shown that 40.41 % of particles with their density being 2000 kg/m^3 and diameter $10 \text{ }\mu\text{m}$ deposited in the analyzed section of the airways under the inspiratory flow rate being 15 L/min; under 30 L/min, 80.19 %; under 60 L/min, 99.82 %. Particles with their diameter being $5 \text{ }\mu\text{m}$ and density being 2000 kg/m^3 had the following deposition levels: 15.92 % under the flow rate 15 L/min; 11.63 % under 30 L/min; and 8.88 % under 60 L/min. Also, the authors of [22] reported the results of investigating influence exerted by particle density on effectiveness of their deposition in the airways. Particle density was noted to have a significant effect on differences between deposition of micro-sized particles ($10 \text{ }\mu\text{m}$) and a rather insignificant one on deposition of nano-sized particles (5 nm).

Fewer studies addressed non-stationary respiration. Thus, the authors of [26, 27] investigated non-stationary airflow with micro-sized particles (spherical ones sized between 2 and $30 \text{ }\mu\text{m}$ in the work [26], ellipsoid-like ones sized between 1 and $15 \text{ }\mu\text{m}$ in the work [27]) in the upper airways based on a real geometry (in the section between the nasal cavity and trachea).

The study [16] considered both stationary and non-stationary flow of gas suspension in the airways between the mouth and the fourth generation of the asymmetric trachea-bronchial tree. The authors estimated deposition of micro-sized particles (1, 2, 5, 8, 10, and $15 \text{ }\mu\text{m}$) in the different sections of the airways. They reported the results indicating that a share of deposited particles was lower for smaller fractions and higher for bigger ones under non-stationary airflow against stationary one. Nano-sized particles were not considered in this study.

Non-stationary airflow in the lower airways with a real geometry based on CT scans was investigated in [28]. In this study, a non-stationary inspiratory flow rate was specified at the entry to the trachea. The study reported the results on airflow velocities, airflow pressure on the airway walls; the study did not consider particle motion and deposition in the airways.

Studies that investigate non-stationary respiration usually take laws of changes in inspiratory flow rates at the entry as sinusoidal with different sinusoid amplitudes and periods. It is assumed in the works [26, 27], that one average human respiratory cycle (inhaling and exhaling) takes 4 seconds and inhalation and exhalation last 2 seconds each; an airflow rate at the entry cross-section changes as per sinusoid and reaches its peak value (approximately 20 L/min) in the middle of inhalation. In the study [16], a respiratory cycle is taken as equal to 3.8 seconds, inhalation is about 1.8 seconds. In the study [28], a respiratory cycle lasts 5.1 seconds, inhalation is 1.7 seconds. The authors in the [30] take a respiratory cycle as being 4 seconds long, inhalation is 1.65 seconds. In the study [19], a respiratory cycle is approximately 5 seconds and inhalation lasts about 2.2 seconds. All the laws considered in these aforementioned studies conform to well-known physiological data; although parameters of the sinusoidal law for incoming airflow are different, approximately 0.5 liters of air enter the human body by one calm inhalation under each preset condition.

Airflow character depends on respiration conditions. Under calm respiration, the Reynolds number reaches 2100 in the trachea [31], 1982 [28], 2160 [32]. Airflow can be either laminar or transitional in the lower airways. In the studies [28, 32] airflow was assumed to be laminar; in the studies [31, 33], it was assumed to be transitional and was described with a low-Reynolds turbulence model $k-\omega$. The author of the study [31] points out that airflow is complicated and not laminar in its essence.

Therefore, the present study is accomplished within achieving the general goal, which is to develop the mathematical model of the human respiratory system. In this study, specific attention is paid to investigating non-stationary flow of a multi-phase mixture of gases and solid dust particles with different dispersed structure (macro-, micro-, and nano-sized particles) in the lower airways with a real anatomic shape; another aim is to estimate deposition of dust particles (with different dispersed structure and density) in the airways and the lungs.

CONCEPTUAL STATEMENT

In general case, inhaled air is a multi-phase multi-component mixture of a gases and solid dust particles. Gas exchange does not occur in the airways (the transition phase), a gas has a constant component structure; we shall consider inhaled air as a multi-phase mixture of a homogenous gas and solid dust particles of different sizes.

We apply the Euler–Lagrange approach to simulate multi-phase mixture motion. Motion of a basic carrier gas phase is described using the Euler approach (the viscous flow model). Solid dust particles are a dispersed carried phase, which is described with the material approach. Particles of different sizes are given individual labels (most frequently, numbers); a specific ordinary differential equation (ODE) is written to describe motion of each particle. This equation describes an individual motion path within the velocity field of the carrier phase. In this study, particles are assumed to be spherical. The volume concentration of the dispersed phase (particulate matter) is considerably smaller than the carrier phase (is about 2×10^{-7}); given that, any interactions between particles are neglected.

In general case, when investigating airflow (flow of a multi-phase mixture containing a gas and solid particles) in the lower airways, we should determine the velocity of dispersed phase particles at the entry to the trachea relying on the results obtained by modeling a flow of this mixture in the upper airways. In this study, we use approximation stating that the velocity of dispersed phase particles at the cross-section of the entry to the airways is assumed to be equal to the velocity of the carrier phase.

We investigate airflow in the lower airways starting from the trachea. The trachea is divided into two main bronchi; the right main bronchus is shorter than the left one and seems a natural extension of the trachea [34]. The angle of the left main bronchus where it branches out from the trachea (in the sagittal plane) is bigger than the angle of the right main bronchus [35–37]. The right main bronchus creates the upper, middle, and inferior lobar bronchi; the

left main bronchus creates the upper and inferior lobar bronchi that are then divided into the segmental bronchi.

We investigate airflow in the airways based on an actual anatomic shape typical for an adult person. The geometry of the lower airways based on CT scans was obtained as a stereolithography file (in STL format) from the website of the Pennsylvania State University (PennState) (<https://www.engr.psu.edu/msmlung/#>). The initial geometry was rather rough; it was preliminarily processed using AnsysSpaceClaim: some low-quality artifacts were removed by hand and surface irregularities were smoothed. The ultimate geometry of the lower airways in axonometry (the frontal view) is shown in Figure 1. This geometry belongs to an adult person: the trachea cross-section area is 1.389 cm^2 (this corresponds to a diameter about 13.3 mm); the trachea is approximately 125 mm long. These dimensions conform to the physiological standard for an adult person [34].

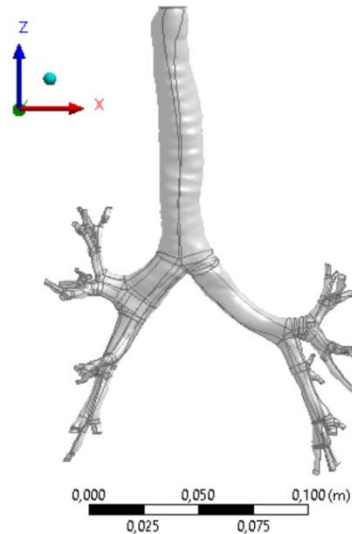


Fig. 1. The three-dimensional geometry of the lower airways based on CT scans, in axonometry (frontal view)

Air is warmed in the upper airways; air warming during respiration was investigated in detail in [11]; based on the data obtained in the aforementioned study, we assume that air temperature is $36.6 \text{ }^\circ\text{C}$ at the entry to the trachea and heat exchange does not occur in the lower airways.

Respiration is a non-stationary process. Air flows due to the difference between the atmospheric pressure and the pressure at the entry to the lungs. Approximately 500 ml of air move into the lungs of a healthy adult per one inhalation (tidal volume); a person makes approximately 15 respiratory cycles per minute [38, 39]. One average human respiratory cycle (inhalation – exhalation) is assumed to last 4 seconds, inhalation and exhalation last 2 seconds each. The constant pressure, which is equal to the atmospheric pressure, is set at the entry to the trachea ($p^{\text{in}} = 101325 \text{ Pa}$). The pressure at the exit from the bronchi is determined as per the periodical law described by the equation $p^{\text{out}} = 101325 - 9 \sin(\frac{\pi}{2}t)$. Under these conditions, an average flow rate amounts to 15 L/min (0.25 L/s) at the entry cross-section during inhalation; 0.5 L of air move into the airways during one inhalation that lasts 2 seconds and this is in line with available literature and experimental data [38, 39]. Figure 2 provides the graph describing the inspiratory flow rate in respiration.

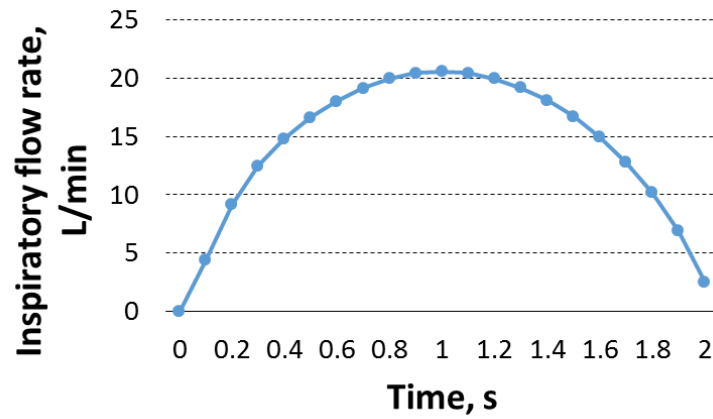


Fig. 2. The graph showing changes in the flow rate at the cross-section of the entry to the trachea during inhalation

Under the periodical boundary conditions specified in this study, minute ventilation corresponds to calm respiration. The flow rate changes between 0 and 20.6 L/min (Figure 2) at the entry to the trachea during one inhalation. A similar regularity of changes in inspiratory flow rates was used in the studies [26, 27], where the authors investigated non-stationary airflow in the upper airways. The initial flow rate is not equal to 0 at 2 seconds due to inertia associated with airflow being non-stationary.

Many studies [24, 22] investigate airflow under a constant inspiratory flow rate at the entry to the airways, which is equal to 15 L/min. The flow rate equal to 15 L/min corresponds to 0.4 and 1.6 seconds from the moment a respiratory cycle starts.

Since we cannot specify actual conditions for a random initial moment of time, we apply some idealized initial conditions: the pressure is homogenous and equal to the atmospheric air pressure at the initial moment ($t = 0$ c) and the airflow velocity is equal to 0. The tangential components of the stress tensor are assumed to be equal to 0 at the entry to the trachea and exits from the bronchi.

The walls of the large airways contain rigid cartilaginous tissue that prevents them from deforming easily. Therefore, we can neglect any deformations of the airways when investigating airflow and particle deposition in the analyzed sections (Figure 1) and assume their walls to be immobile. The surface of the airways is assumed to be covered with a highly viscous layer; when carried solid particles contact it, they lose their velocity and cease moving.

Preliminarily, we calculated airflow in the lower airways assuming it to be laminar. Based on this calculation, we estimated the inspiratory flow rates (L/min) and the Reynolds numbers, which tend to reach approximately 2300 during non-stationary respiration and this value is a critical threshold one. We applied the $k-\omega$ model [40] to describe transition airflow; it has been established to be quite relevant for modeling internal flows along curved channels with small volumes and makes it possible to calculate near-wall turbulence.

MATHEMATICAL STATEMENT

When modeling dust-containing airflow in the lower airways, we apply a reference system (RS) associated with the human body and assumed to be inertial (due to inertia forces being too small in comparison with other mechanical impacts). The carrier phase motion (identified with the subscript 1) is described with the mass and impulse preservation equations:

$$\frac{\partial \rho_{(1)}}{\partial t} + \nabla \cdot (\rho_{(1)} \mathbf{v}_{(1)}) = 0, \quad \mathbf{r} \in \Omega, \quad t \in (0; T], \quad (1)$$

$$\frac{\partial}{\partial t}(\rho_{(1)} \mathbf{v}_{(1)}) + \nabla \cdot (\rho_{(1)} \mathbf{v}_{(1)} \mathbf{v}_{(1)}) = \nabla \cdot \boldsymbol{\sigma}_{(1)} + \rho_{(1)} \mathbf{g} - \sum_j \mathbf{P}_{(1)(j)}, \quad \mathbf{r} \in \Omega, t \in (0; T], \quad (2)$$

here $\rho_{(1)}$ is the air (carrier phase) density, kg/m^3 ; $\mathbf{v}_{(1)}$ is the vector of the carrier phase velocity, m/s ; $\boldsymbol{\sigma}_{(1)}$ is the Cauchy stress tensor for the carrier phase, Pa ; \mathbf{g} is the mass force vector, m/s^2 ; $\mathbf{P}_{(1)(j)}$ is the member that describes the intensity of impulse exchange between the first and j -th phases, N/m^3 ; \mathbf{r} is the radius vector, t is time, Ω is the internal area of the airways; Γ is the boundary of the airways (wall); Γ^{in} , Γ^{out} are the boundaries of the entry to and exit from the airways; $\bar{\Omega} = \Omega \cup \Gamma \cup \Gamma^{\text{in}} \cup \Gamma^{\text{out}}$ is the closed area.

The relationship for the Cauchy stress tensor is written as:

$$\boldsymbol{\sigma}_{(1)} = -p_{(1)} \mathbf{I} + \hat{\boldsymbol{\tau}}_{(1)}, \quad \mathbf{r} \in \bar{\Omega}, t \in (0; T], \quad (3)$$

where $p_{(1)}$ is the carrier phase pressure, Pa ; \mathbf{I} is the identity tensor, Pa ; $\hat{\boldsymbol{\tau}}_{(1)}$ is the deviator of the Cauchy stress tensor for the carrier phase.

The deviator of the Cauchy stress tensor is identified as per the following relationship [40]:

$$\hat{\boldsymbol{\tau}}_{(1)} = \mu_{(1)} \left[\nabla \mathbf{v}_{(1)} + (\nabla \mathbf{v}_{(1)})^T - \frac{2}{3} \mathbf{I} \nabla \cdot \mathbf{v}_{(1)} \right] + \boldsymbol{\tau}_{(1)}, \quad \mathbf{r} \in \bar{\Omega}, t \in (0; T], \quad (4)$$

where $\mu_{(1)}$ is the dynamic viscosity of the carrier phase, $\text{Pa}\cdot\text{s}$; $\boldsymbol{\tau}_{(1)}$ is the Reynolds stress tensor (Pa), which is identified as per the following relationship:

$$\boldsymbol{\tau}_{(1)} = \mu_{T(1)} \left[\nabla \mathbf{v}_{(1)} + (\nabla \mathbf{v}_{(1)})^T - \frac{2}{3} \mathbf{I} \nabla \cdot \mathbf{v}_{(1)} \right] - \frac{2}{3} \rho k \mathbf{I}, \quad \mathbf{r} \in \bar{\Omega}, t \in (0; T], \quad (5)$$

where $\mu_{T(1)}$ is the eddy viscosity, $\text{Pa}\cdot\text{s}$ ($\mu_{T(1)} = \rho_{(1)} \frac{k}{\omega}$); k is the kinetic energy of turbulence per a mass unit, J/kg ; ω is the specific dissipation rate for turbulence energy per an energy unit, s^{-1} .

The spherical Cauchy stress tensor is identified considering the equation (1) as per the following relationship:

$$p_{(1)} = \rho_{(1)} R \theta_{(1)}, \quad \mathbf{r} \in \bar{\Omega}, t \in (0; T], \quad (6)$$

where $\theta_{(1)}$ is the carrier phase temperature, Celsius degrees $^{\circ}\text{C}$ (is taken as constant and equal to 36.6°C); R is the molar gas constant.

To describe turbulent airflow, we apply relationships for kinetic turbulence energy and the specific dissipation rate for turbulence energy of the k - ω model:

$$\frac{\partial}{\partial t}(\rho_{(1)} k) + \nabla \cdot (\rho_{(1)} \mathbf{v}_{(1)} k) = \nabla \cdot \left(\left(\mu_{(1)} + \frac{\mu_{T(1)}}{\sigma_k} \right) \nabla k \right) + P_k - \beta' \rho_{(1)} k \omega; \quad \mathbf{r} \in \bar{\Omega}, t \in (0; T], \quad (7)$$

$$\frac{\partial}{\partial t}(\rho_{(1)} \omega) + \nabla \cdot (\rho_{(1)} \mathbf{v}_{(1)} \omega) = \nabla \cdot \left(\left(\mu_{(1)} + \frac{\mu_{T(1)}}{\sigma_w} \right) \nabla \omega \right) + \alpha \frac{\omega}{k} P_k - \beta \rho_{(1)} \omega^2, \quad \mathbf{r} \in \bar{\Omega}, t \in (0; T], \quad (8)$$

where P_k is the member to describe how turbulence occurs due to viscous forces; α , β , β' , σ_k , σ_w are the turbulence model parameters ($\sigma_k = 1$; $\sigma_w = 1$).

The motion of the dispersed carried phase particles ($j = \overline{2, J}$) is described with the Newton's Second Law that considers the gravity force and the force determined by impacts of slip airflow:

$$m_{(j)} \frac{d\mathbf{v}_{(j)}}{dt} = m_{(j)} \mathbf{g} + \frac{1}{8} \rho_{(j)} \pi d_{(j)}^2 C_D |\mathbf{v}_{(1)} - \mathbf{v}_{(j)}| (\mathbf{v}_{(1)} - \mathbf{v}_{(j)}), \quad \mathbf{r}_{(j)} \in \bar{\Omega}, t \in (0; T], \quad (9)$$

where $\mathbf{v}_{(j)}$ is the velocity of the center of gravity for the j -th particle, m/s ($\mathbf{v}_{(j)} = \frac{d\mathbf{r}_{(j)}}{dt}$); $\mathbf{r}_{(j)}$ is the radius-vector of the j -th particle's center of gravity; $m_{(j)}$ is the mass of the j -th particle, kg ($m_{(j)} = \frac{\pi}{6} d_{(j)}^3 \rho_{(j)}$); $\rho_{(j)}$ is the density of the j -th particle, kg/m³; $d_{(j)}$ is the diameter of the j -th particle; C_D is the resistance coefficient to describe resistance to airflow; it is identified for spherical particles as per the relationship [41]:

$$C_D = \max\left(\frac{24}{\text{Re}}(1 + 0.15 \text{Re}^{0.687}), 0.44\right) \quad \text{Re} = \frac{|\mathbf{v}_{(1)} - \mathbf{v}_{(j)}| d_{(j)}}{v_{(1)}}, \quad (10)$$

where Re is the Reynolds number.

The initial conditions for the velocity of the multi-phase mixture and the carrier phase pressure are written as follows:

$$\mathbf{v}_{(1)}(0, \mathbf{r}) = \mathbf{0}, \quad \mathbf{r} \in \bar{\Omega}, t = 0, \quad (11)$$

$$\mathbf{v}_{(j)}|_{\Gamma^{\text{in}}} = \mathbf{0}, \quad \mathbf{r}_{(j)} \in \Gamma^{\text{in}}, t = 0, \quad (12)$$

$$p_{(1)}(0, \mathbf{r}) = p^{\text{in}}, \quad \mathbf{r} \in \bar{\Omega}, t = 0. \quad (13)$$

The boundary conditions include the relationships at the entry (Γ^{in}), exits (Γ^{out}) and walls of the airways (Γ). Static boundary conditions are specified at the entry (Γ^{in}) to and exits from (Γ^{out}) the airways:

$$\mathbf{n} \cdot \boldsymbol{\sigma}_{(1)} \cdot \mathbf{n} = p^{\text{in}}, \quad \mathbf{n} \cdot \boldsymbol{\sigma}_{(1)} - (\mathbf{n} \cdot \boldsymbol{\sigma}_{(1)} \cdot \mathbf{n}) \mathbf{n} = \mathbf{0}, \quad \mathbf{r} \in \Gamma^{\text{in}}, t \in (0; T], \quad (14)$$

$$\mathbf{n} \cdot \boldsymbol{\sigma}_{(1)} \cdot \mathbf{n} = p^{\text{out}}, \quad \mathbf{n} \cdot \boldsymbol{\sigma}_{(1)} - (\mathbf{n} \cdot \boldsymbol{\sigma}_{(1)} \cdot \mathbf{n}) \mathbf{n} = \mathbf{0}, \quad \mathbf{r} \in \Gamma^{\text{out}}, t \in (0; T]. \quad (15)$$

Introduction of different particle fractions is specified at the entry cross-section according to the even distribution law (in terms of statistics) under specified average inputs. The particle velocity is assumed to be equal to the carrier gas phase velocity at the entry to the trachea:

$$\mathbf{v}_{(j)}|_{\Gamma^{\text{in}}} = \mathbf{v}_{(1)}, \quad \mathbf{r}_{(j)} \in \Gamma^{\text{in}}, t \in (0; T], \quad (16)$$

The no-slip condition is specified at the airway walls (Γ):

$$\mathbf{v}_{(1)}|_{\Gamma} = \mathbf{0}, \quad \mathbf{r} \in \Gamma, t \in (0; T], \quad (17)$$

The condition for deposition of particles (the carried phase, $j = \overline{2, J}$) on the airway walls (Γ) is written as:

$$(\mathbf{r}_{(j)} \in \Gamma) \cap (\mathbf{n} \cdot \mathbf{v}_j < 0), \quad j = \overline{2, J}, t \in (0; T] \quad (18)$$

In case the condition (18) is met for a certain particle, we fix coordinates of the point where it came into a contact with the airway wall and this particle is no longer considered in motion.

RESULTS

We calculated properties of the non-stationary airflow (a multi-phase mixture of gases and dust particles) in the lower airways using Ansys CFX software package. During inhalation, the flow rate at the cross-section of the entry to the trachea changes between 0 and

20.6 L/min; the airflow velocity changes between 0 and 3.95 m/s and reaches its peak at the moment that corresponds to the middle on inhalation. At this moment, we observe the greatest difference between the pressures at the entry to and exit from the airways and the greatest incoming airflow rates (1 second from the start of a respiratory cycle). Figure 3 provides a graph showing changes in the average airflow velocity (the carrier phase) at the cross-section of the entry to the airways. Under the specified boundary conditions, the average airflow velocity at the entry to the trachea reaches 2.47 m/s 1 second after the start of a respiratory cycle.

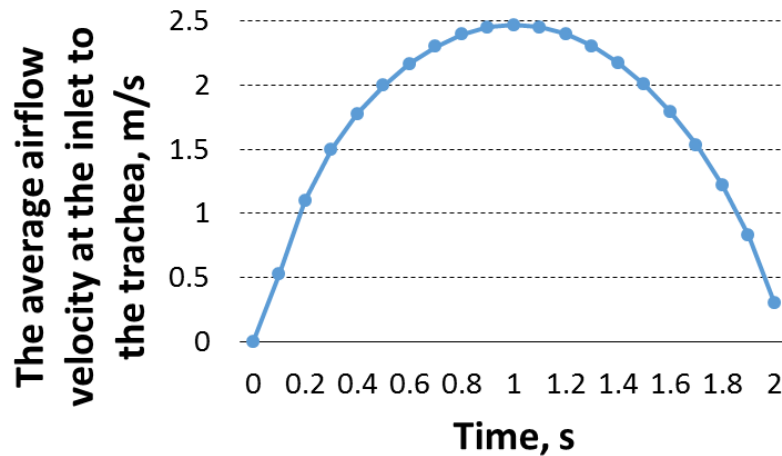


Fig. 3. The average airflow velocity at the entry to the airways

Figures 4a–4d present airflow velocity streamlines at different moments during inhalation.

The highest airflow velocities are detected in the trachea (at the anterior wall). The airflow mainstream goes along the trachea into the right main bronchus. This is due to anatomic features of the airways: the right main bronchus is shorter and wider than the left one and is considered a natural extension of the trachea; it branches out from the trachea at a lesser angle [34]. Turbinal airflow occurs in the trachea in addition to the mainstream moving along the trachea right wall. This turbinal airflow occurs in the middle of the trachea near its left and anterior wall and moves towards the point where the trachea divides into the main bronchi.

The particle velocity in the main stream in the trachea varies between 2 and 3 m/s at the time moment 1 s after the start of a respiratory cycle (when the airflow velocities are the highest). The particle velocity in the turbinal stream is lower and does not exceed 1 m/s. The airflow velocity is also lower in the main bronchi and smaller ones (it varies between 1 and 2 m/s). Airflow turbulences occur in the section around the middle of the trachea along its left wall, near the entry to the left main bronchus, at the place where the right main bronchus branches into the middle and inferior lobar bronchi and near the walls.

Generally, as airway diameters become smaller, airflow velocities decrease. Airflow is calmer in the smaller airways and only insignificant turbulences occur at places where bronchi branch out.

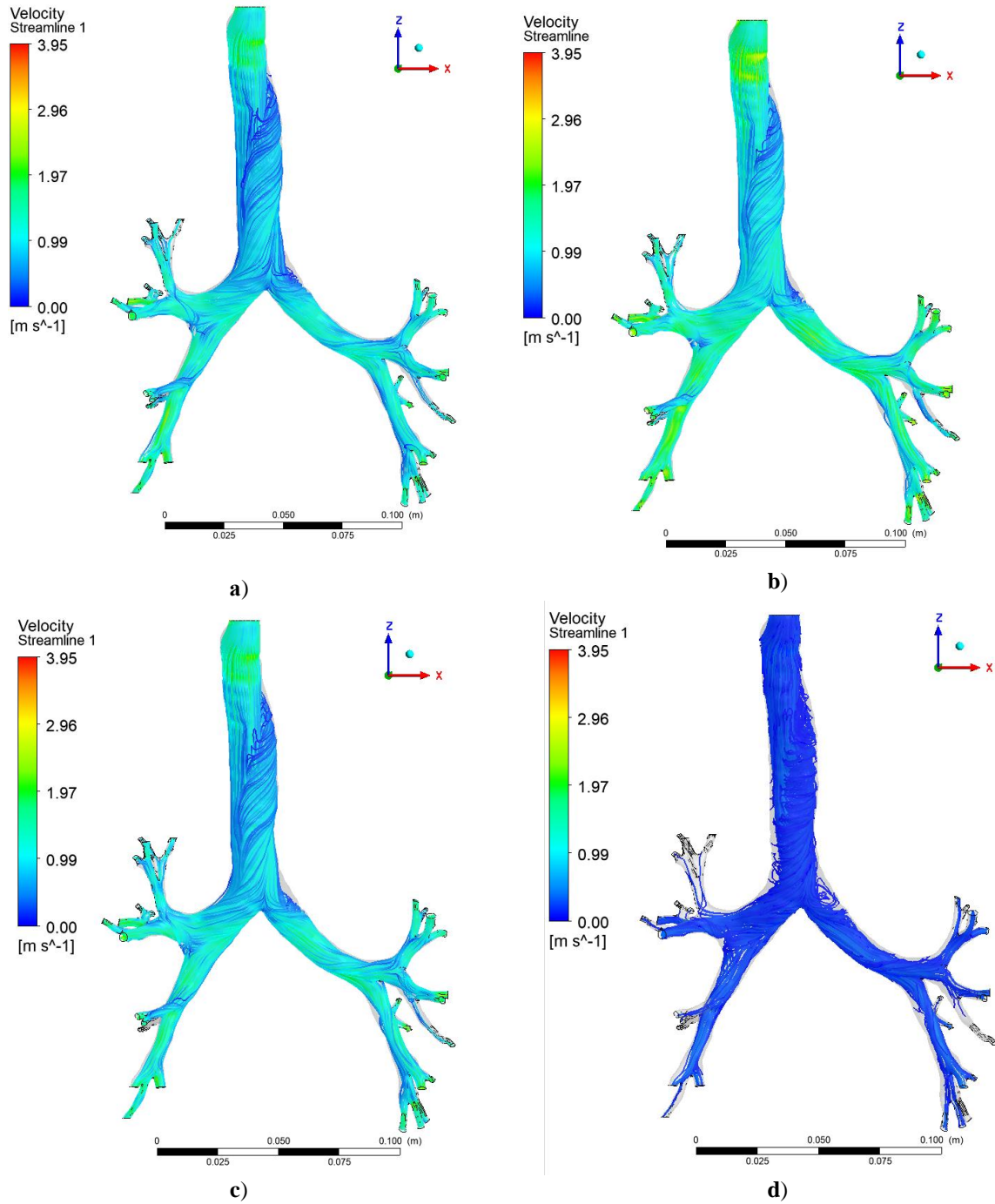


Fig. 4. The airflow velocity streamlines in the lower airways (frontal view) at the moment **a)** $t = 0.5$ s after a respiratory cycle starts; **b)** $t = 1$ s after a respiratory cycle starts; **c)** $t = 1.5$ s after a respiratory cycle starts; **d)** $t = 2$ s after a respiratory cycle starts

In this study, we examined motion and deposition of dust particles with different density and dispersed structures (macro-, micro-, and nano-sized particles) in the lower airways. We considered particles with different densities, 1000, 2000 and 2700 kg/m³, and diameters varying between 10 nm and 100 μ m. Figures 5a–5d provide the results obtained by investigating particle motion (their density is 2000 kg/m³) in the airways, namely, motion paths identified for particles of different sizes contained in inhaled air.

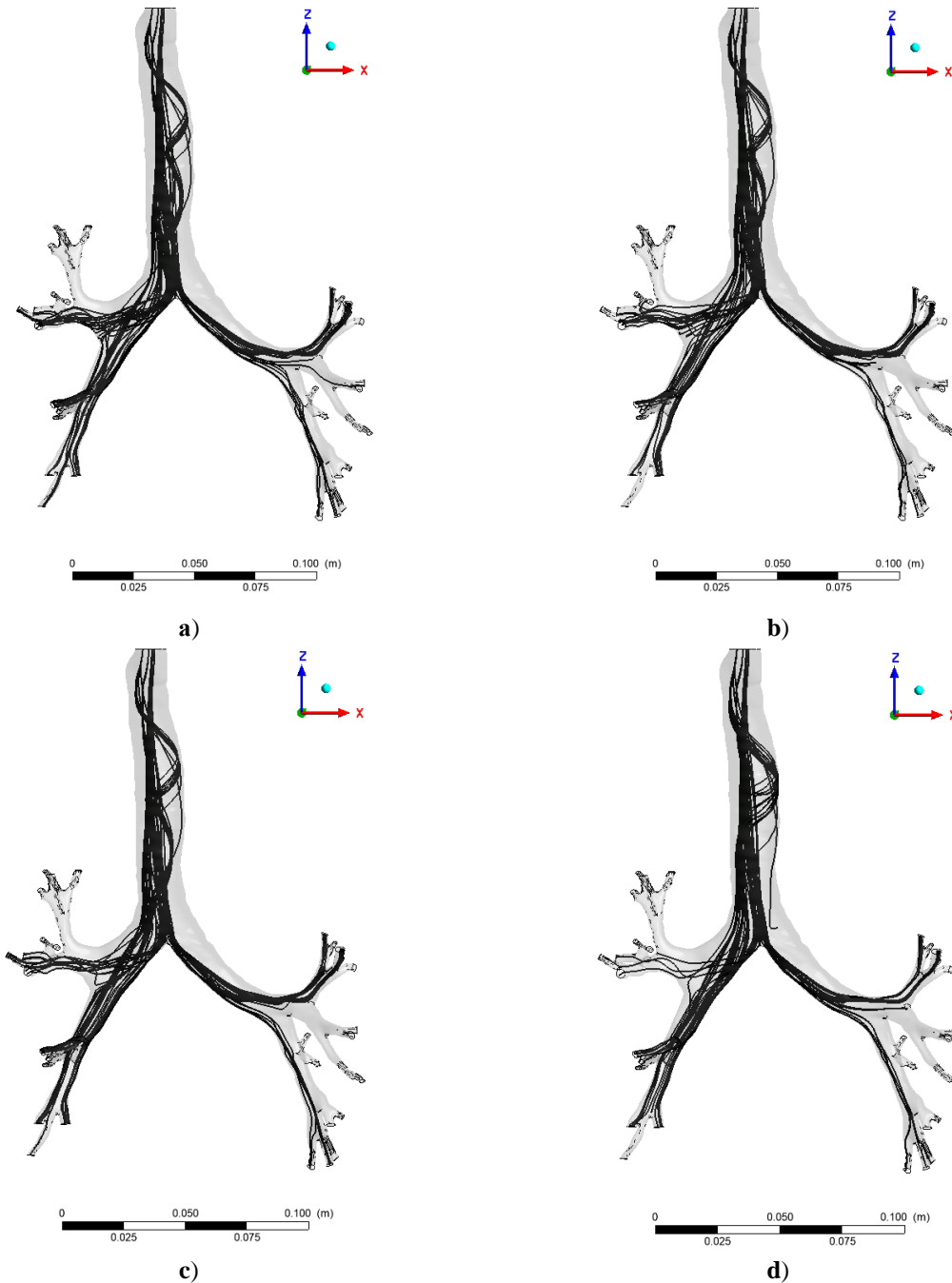


Fig. 5. The motion paths of solid particles sized: **a)** 1 μm ; **b)** 2.5 μm ; **c)** 5 μm ; **d)** 10 μm

Obviously, the smaller is the size, the more particles reach the lower airways. Particles sized 1 μm or smaller move together with airflow; motion of such particles appears to be turbinal in the trachea (especially in the section between the middle of the trachea along the left wall and the entry to the left main bronchus). Particles of such sizes hardly deposit in the trachea; their insignificant deposition occurs at the place where the trachea branches out to the left main bronchus and at places where smaller airways branch out. The major part of such particles reaches smaller airways and the lungs. Motion paths of nano-sized particles almost coincide with those of particles sized 1 μm and with the motion path of the carrier gas phase.

The greater is the size, the more particles deposit. Thus, particles sized 2 μm start to deposit at the place where the trachea divides into the main bronchi and at the places where the lobar bronchi branch out; the share of particles able to reach smaller airways goes down.

Particles sized 5 μm follow motion paths similar to those of particles sized 2.5 μm but a bigger share of such particles deposits at the place where the main bronchi branch out.

Particles sized 10 μm deposit already in the trachea and at the place where the left main bronchus branches out; the share of particles that deposit at the places where the airways branch out goes up.

It is noteworthy that, according to numeric modeling results, dust particles mostly penetrate the right main bronchus, predominantly the middle and inferior lobar bronchi, which enter the right middle lobe and the right lower lobe accordingly. The smallest quantity of particles with all analyzed sizes penetrates the right upper lobar bronchus.

Particulate matter produces fibrogenic effects. Accumulation of insoluble dust particles in the lungs may induce pneumoconiosis (silicosis, etc.). The disease has a particular feature; namely, it typically involves developing pneumosclerosis (diffuse fibrosis of the lungs when the connective tissue grows and cicatricial deformities occur). Overgrowing connective tissue in the lungs disrupts proper respiration, makes the alveolar-capillary membranes thicker and flatter, reduces the lung tissue permeability and decreases an effective gas exchange area.

X-ray study is the basic method to diagnose silicosis. At its initial stage, x-ray images show enhancement and deformations of a lung pattern; as a rule, these changes are symmetrical or sometimes more apparent in the right lung and predominantly localized in the middle and lower lobes [42, 43]. The particle deposition patterns identified by numeric methods are quite consistent with this medical fact.

The calculations made it possible to quantify deposition of particles with different densities and dispersed structures in the human airways. The share of deposited particles was determined as a ratio of particles deposited on the airway walls to the total number of particles that penetrated the airways. Figure 6 and Table 1 provide data on shares of deposited particles (%) depending on their diameter (from 10 nm to 100 μm), the densities being 1000, 2000, and 2700 kg/m^3 .

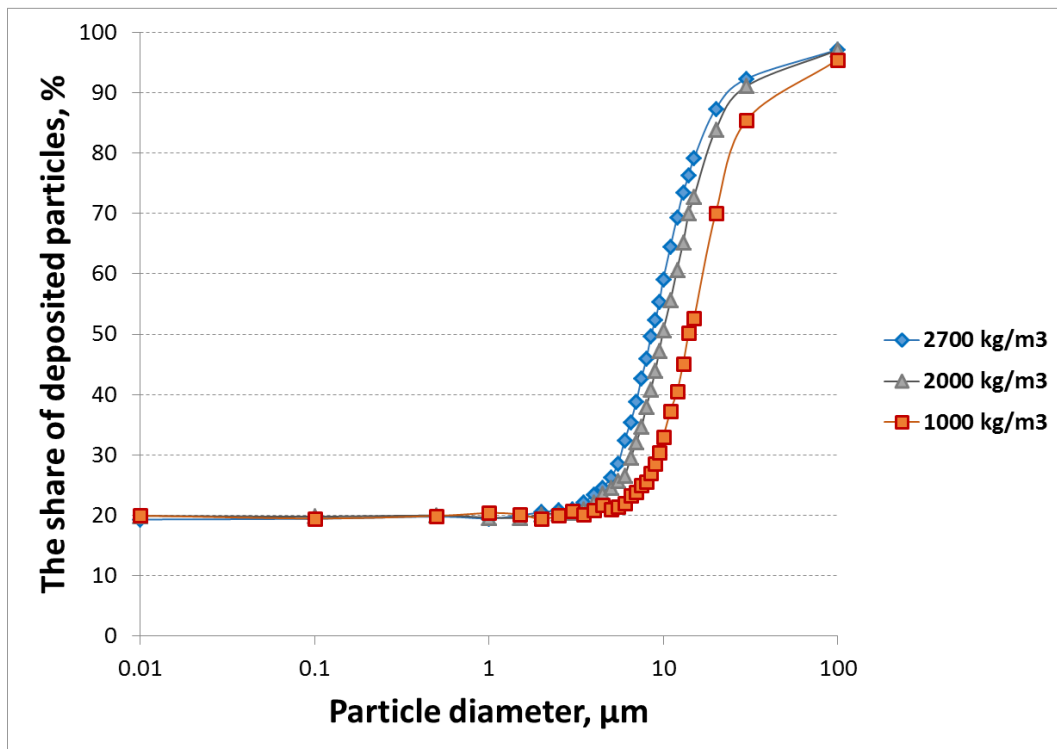


Fig. 6. The shares of particles with different dispersed structure that deposit in the human lower airways, %

The function graph for the share of deposited particles depending on their diameters is an S-shape (sigmoid) function. Large particles (bigger than 10 μm) with a heavy mass almost completely deposit in the airways. As particle sizes and mass go down, the share of particles depositing in the airways decreases and accordingly there is a growth in the share of particles able to penetrate small airways and reach the lungs.

Particles with their diameter 1 μm or smaller have similar motion paths as they move along with the carrier phase flow. Deposition of small particles barely depends on density: the share of deposited particles with such sizes is almost constant and equal to approximately 20 % of all the particles that reach the entry to the trachea. Density of a material mostly influences the share of deposited micro-sized particles (from 2.5 to 20 μm). The greater is the density, the bigger share of them deposits in the airways.

Table 1 provides quantitative assessments of particle deposition in the lower airways depending on their dispersed structure for three materials with different density.

Table 1. Deposition of dust particles with different dispersed structure in the lower airways with a real anatomic shape

Diameter, μm	Share of deposited particles, %		
	1000 kg/m^3	2000 kg/m^3	2700 kg/m^3
0.01	19.96	19.93	19.32
0.1	19.50	19.82	19.46
0.5	19.94	19.98	19.80
1	20.41	19.64	19.49
1.5	20.16	19.60	20.03
2	19.38	20.15	20.52
2.5	20.04	20.36	20.84
3	20.71	20.42	21.02
3.5	20.18	20.96	22.19
4	20.85	22.13	23.37
4.5	21.76	23.56	24.55
5	20.96	24.55	26.29
5.5	21.45	25.69	28.50
6	21.96	26.57	32.37
6.5	23.30	29.49	35.46
7	23.86	32.13	38.79
7.5	25.04	34.69	42.72
8	25.62	37.99	45.89
8.5	26.92	40.85	49.70
9	28.59	43.98	52.32
9.5	30.37	47.28	55.39
10	32.99	50.59	59.09
11	37.32	55.62	64.54
12	40.49	60.69	69.35
13	45.14	65.18	73.45
14	50.16	70.09	76.29
15	52.61	72.79	79.17
20	70.09	83.89	87.33
30	85.42	91.06	92.28
100	95.46	97.05	97.12

Density of a material mostly influences differences between shares of deposited micro-sized particles. Thus, 26.29 % of particles with density equal to 2700 kg/m^3 deposit in the lower airways; 24.55 % of particles with density equal to 2000 kg/m^3 ; 20.96 % of particles with density equal to 1000 kg/m^3 (Table 1). Among particles sized 10 μm , 59.09 % of particles with their density equal to 2700 kg/m^3 deposit in the lower airways; 50.59 % of the particles with their density equal to 2000 kg/m^3 ; 32.99 % of particles with their density equal to 1000 kg/m^3 .

The hygienic standards that are valid in the Russian Federation at the moment aim to control the total suspended particulate (TSP), particulate matter sized 10 μm (PM_{10}), and

particulate matter sized 2.5 μm (PM_{2.5}) in ambient air¹. Still, the existing standards do not consider a material of particulate matter. Numeric modeling clearly indicates there are differences in shares of particles depositing in the airways depending on their density. This may give grounds for revising the existing hygienic standards. They should cover not only sizes and levels of particulate matter but particle density as well.

Numeric calculations of airflow that contains particulate matter in various concentrations have revealed that the share of particles (of a certain size) deposited in the airways is constant and does not depend on an incoming concentration. However, the latter influences the total quantity of particles penetrating the human body and, accordingly, their ability to induce respiratory diseases.

DISCUSSION

The results of this study are consistent with some other research works. The law of changes in airflow rates at the cross-section of the entry to trachea, which we applied in this study, is similar to the law described in the works [26, 27] with their focus on non-stationary airflow in the upper airways from the entry to the nasal cavity to the exit from the trachea. It is also consistent with experimental data reported in [39]. Data on a lung volume per one inhalation are in line with well-known medical data [38, 39] and data of mathematical models describing the respiratory system [29, 30, 19].

The calculated airflow velocities in the lower airways are in line with the results reported in [29, 32, 19]. According to numeric modeling, the airflow velocity changes between 0 and 3.95 m/s during respiration (the airflow rate is 0–20.6 L/min). The airflow velocity at the entry to the trachea changes between 0 and 2.47 m/s at the start of a respiratory cycle; the airflow velocity in the trachea is between 2 and 3 m/s in the middle of inhalation (time interval is 0.5–1.5 s). In the study [29], the airflow velocity reaches 6.6 m/s (the incoming airflow rate reaches 30 L/min during respiration); the airflow velocity varies between 2 and 3 m/s in the trachea.

The study [32] addressed airflow in the lower airways of three healthy people and six people with pathologies. Under the constant airflow rate being 27.7 L/min (0.462 L/s), the airflow velocity at the entry to a healthy person's trachea varies between 1.52 and 2.85 m/s (depending on an individual entry sectional area) [32]. The airflow velocity reaches 4.27, 5.04, or 6.01 m/s in the lower airways depending on their individual shape. The velocity values are consistent and differences are determined by individual features of the airways specified by boundary conditions and occurring inertia associated with non-stationary airflow, which is considered in this study.

Reynolds number values reach 2234 at the cross-section of the entry to the trachea (at the time moment corresponding to the airflow rate at the entry to the trachea equal to 0.34 L/s); this is quite consistent with the results reported in the study by Luo and Liu [31] ($Re = 2100$ at the entry airflow rate being 0.44 L/s) that was accomplished using a low-Reynolds turbulence model $k-\omega$. Different values are probably due to a smaller area of the entry cross-section and, accordingly, a higher velocity under the same airflow rate in the geometry of the airways considered by the authors in this work. Reynolds numbers reach 2700 in the trachea; given that, we can consider transitional airflow in the airways under non-stationary airflow already under calm respiration. Reynolds numbers are likely to be higher under more active respiration. In the study [29], Reynolds numbers reached 1982 at the entry to the trachea under non-stationary calm respiration but the considered airflow was assumed to be laminar and a turbulence model was not used.

¹Safe Standards GN 2.1.6.2604-10 Maximum Permissible Concentrations (MPC) of Pollutants in Ambient Air in Settlements. Supplement No. 8 to GN 2.1.6.1338-03, approved in 2010 by the Order of the RRF Chief Sanitary Inspector dated April 19, 2010 No. 26.

Our results concerning particle deposition depending on their density coincide with findings reported in the study [22] about particle density being able to influence differences in deposition of micro-sized particles (10 μm) and not having any effects on deposition of nano-sized ones (5 nm); still there are some differences from quantitative estimates of deposition obtained in our study. Thus, it was shown in [22], that 9–16 % of nano-sized particles (5 nm) entering the body through the mouth deposited in the airways depending on respiration (16 % deposited of the entry airflow rate was 15 L/min). In our study, we established that approximately 20 % of nanoparticles sized 10 nm deposited in the lower airways in case they were able to reach the trachea. These differences occur since our study focused on investigating non-stationary airflow under different entry airflow rates (within the range between 0 and 20.6 L/min in our study (the average airflow rate is 15 L/min); 15, 30, and 60 L/min in [22]); in addition, we did not consider the share of particles deposited in the oral cavity, oral pharynx and larynx in our study.

We established in this study that 50.59 % of particles sized 10 μm and with density 2000 kg/m^3 and 32.99 % of particles with density 1000 kg/m^3 deposited in the lower airways. The authors of the study [22] reported that 40.41 % of particles with density 2000 kg/m^3 and 30.31 % of particles with density 1120 kg/m^3 deposited under the entry airflow rate being 15 L/min. The differences between these results are likely due to us considering non-stationary airflow in our study. If the average entry airflow rate is 15 L/min, the total airflow rate reaches higher values (up to 20.6 L/min in the middle of inhalation) and this influences effectiveness of particle deposition.

According to the findings reported in [21], 12–16 % of particles sized 2.5 μm and density 1200 kg/m^3 deposited in the section of the airways between the oral cavity and segmental bronchi under the entry airflow rate equal to 20 L/min; 16–21 % of particles sized 5 μm ; 51–52 % of particles sized 10 μm ; 95 % of particles sized 20 μm ; 99.7 % of particles sized 30 μm . In our study, 20.04 % of particles sized 2.5 μm and with density 1000 kg/m^3 deposited in the same area; 20.96 % of particles sized 5 μm ; 32.99 % of particles sized 10 μm ; 70.06 % of particles sized 20 μm ; 85.42 % of particles sized 30 μm . These values are quite similar in two studies with some slight quantitative differences.

According to the numeric modeling results, the greatest share of inhaled particles enters the right main bronchus, predominantly the middle and inferior lobar bronchi. When entering the airways, dust particles are able to induce lung diseases, pneumoconiosis included. Bacterial agents / pathogenic microorganisms that enter the human body with inhaled air and dust particles contribute to the development of pneumonia. When silicosis is diagnosed, x-ray images show enhancement and deformations of the lung pattern at its initial stage; as a rule, these changes are sometimes more apparent in the right lung and predominantly localized in the middle and lower lobes [42–44]. It is exactly these sections of the airways where most motion paths of particles go to according to our results of numeric modeling.

The results of deposition modeling largely depend on respiration (specified boundary conditions). Our study has a limitation since we specified the same law of changes in pressure at all the exits from the bronchi. In reality, the law of changes in pressure can be different and can change depending on changes in the configuration of different lung sections. At present, we are developing a sub-model to described deformed human lungs; this model can be used, among other things, to establish the law of changes in pressure at the exits from the bronchi / the entries to the lungs [13]. Another limitation is that this study does not consider a share of particles depositing in the upper airways. Particle deposition in the upper airways was investigated in [11].

CONCLUSION

Therefore, the study presents a model that was used to perform numeric investigation of non-stationary airflow with solid particles as well as deposition of particles with different dispersed structure in the human lower airways with an actual anatomic shape. The study

provides images of inhaled airflow streamlines in the lower airways at different moments during inhalation. We have quantified shares of deposited particles with different dispersed structure (from 10 nm to 100 μm) and density (1000 kg/m^3 , 2000 kg/m^3 , 2700 kg/m^3) in the lower airways; the study also contains data on motion paths identified for particulate matter.

The following conclusions can be made based on the study findings:

1) Large particles (larger than 10 μm) and with a heavy mass deposit in the airways almost completely. As a particle size and mass decrease, the share of particles deposited in the airways goes down as well and, accordingly, there is a growth in shares of particles able to reach smaller airways and the lungs.

2) Particles sized 1 μm and smaller move in a similar way and have similar motion paths; they move with the carrier phase flow along airflow streamlines. Deposition of small particles hardly depends on density; the share of deposited particles with such sizes is almost constant and equal to approximately 20 % of all the particles able to reach the entry to the trachea.

3) Particle density mostly influences differences in deposition of micro-sized particles (2.5–20 μm). As particle density and mass grow, the share of particles depositing in the airways also increases due to particle deposition inertia.

4) In the Russian Federation, the existing safe standards aim to control levels of total suspended particles, and specifically particulate matter sized 10 μm and 2.5 μm in ambient air. They do not consider a material particulate matter is made of. Our numeric modeling results that clearly indicate differences in the share of particles depositing in the airways depending on their density can prove that the existing safe standards are to be revised. These standards should cover not only sizes and concentrations but density of particulate matter as well.

5) According to the numeric modeling results, a big share of inhaled dust particles (especially with their diameter being bigger than 1 μm) enters the right main bronchus, predominantly the middle and inferior lobar bronchi. When entering the airways, dust particles are able to induce lung diseases, pneumoconiosis included. The research results are consistent with the fact that x-ray images made to diagnose the diseases usually contain rounded or linear low-density opacities that are located predominantly in the lateral segments of the lungs and mostly in the right lung [42–44].

The further development of the model involves investigating airflow in the deformed human lungs as well as predicting diseases caused by exposure to harmful environmental factors, air dustiness included.

This research was funded by Ministry of Science and Higher Education of the Russian Federation (Project Number FSNM-2023-0003).

REFERENCES

1. Yin P., Brauer M., Cohen A.J., Wang H., Li J., Burnett R.T., Stanaway J.D., Causey K., Larson S., Godwin W., Frostad J., Marks A., Wang L., Zhou M., Murray C.J.L. The effect of air pollution on deaths, disease burden, and life expectancy across China and its provinces, 1990-2017: an analysis for the Global Burden of Disease Study 2017. *Lancet Planet Health*. 2020. V. 4. № 9. P. e386–e398. doi: [10.1016/S2542-5196\(20\)30161-3](https://doi.org/10.1016/S2542-5196(20)30161-3)
2. Rakitskii V.N., Avaliani S.L., Novikov S.M., Shashina T.A., Dodina N.S., Kislitsin V.A. Health risk analysis related to exposure to ambient air contamination as a component in the strategy aimed at reducing global non-infectious epidemics. *Health Risk Analysis*. 2019. V. 4. P. 30–36. doi: 10.21668/health.risk/2019.4.03.eng
3. WHO global air quality guidelines: Particulate matter ($\text{PM}_{2.5}$ and PM_{10}), ozone, nitrogen dioxide, sulfur dioxide and carbon monoxide. Geneva: World Health Organization. 2021. PMID: 34662007. URL: <https://pubmed.ncbi.nlm.nih.gov/34662007/> (accessed 23.03.2026).

4. Xing Y.-F., Xu Y.-H., Shi M.-H., Lian Y.-X. The impact of PM_{2.5} on the human respiratory system. *Journal of Thoracic Disease*. 2016. V. 27. № 1. P. E69–E74. doi: [10.3978/j.issn.2072-1439.2016.01.19](https://doi.org/10.3978/j.issn.2072-1439.2016.01.19)
5. Maji K.J., Dikshit A.K., Arora M., Deshpande A. Estimating premature mortality attributable to PM_{2.5} exposure and benefit of air pollution control policies in China for 2020. *Sci. Total Environ.* 2018. V. 612. P. 683–693. doi: [10.1016/j.scitotenv.2017.08.254](https://doi.org/10.1016/j.scitotenv.2017.08.254)
6. Tikhonova I.V., Zemlyanova M.A., Kol'dibekova Yu.V., Peskova E.V., Ignatova A.M. Hygienic assessment of aerogenic exposure to particulate matter and its impacts on morbidity with respiratory diseases among children living in a zone influenced by emissions from metallurgic production. *Health Risk Analysis*. 2020. V. 3. P. 61–69. doi: [10.21668/health.risk/2020.3.07.eng](https://doi.org/10.21668/health.risk/2020.3.07.eng)
7. Grzywa-Celińska A., Krusiński A., Milanowski J. 'Smoging kills' - Effects of air pollution on human respiratory system. *Ann. Agric. Environ. Med.* 2020. V. 27. № 1. P. 1–5. doi: [10.26444/aaem/110477](https://doi.org/10.26444/aaem/110477)
8. Wei T., Chen C., Yang Y., Li L., Wang J., Ye M., Kan H., Yang D., Song Y., Cai J., Hou D. Associations between short-term exposure to ambient air pollution and lung function in adults. *J. Expo. Sci. Environ. Epidemiol.* 2023. doi: [10.1038/s41370-023-00550-0](https://doi.org/10.1038/s41370-023-00550-0)
9. Adamkiewicz G., Liddie J., Gaffin J.M. The Respiratory Risks of Ambient/Outdoor Air Pollution. *Clin. Chest Med.* 2020. V. 41. № 4. P. 809–824. doi: [10.1016/j.ccm.2020.08.013](https://doi.org/10.1016/j.ccm.2020.08.013)
10. Trusov P.V., Zaitseva N.V., Tsinker M.Yu. Modeling of human breath: conceptual and mathematical statements. *Mathematical Biology and Bioinformatics*. 2016. V. 11. No. 1. P. 64–80 (in Russ.). doi: [10.17537/2016.11.64](https://doi.org/10.17537/2016.11.64)
11. Trusov P.V., Zaitseva N.V., Tsinker M.Yu., Nekrasova A.V. Mathematical model of airflow and solid particles transport in the human nasal cavity. *Mathematical Biology and Bioinformatics*. 2021. V. 16. № 2. P. 349–366 (in Russ.). doi: [10.17537/2021.16.349](https://doi.org/10.17537/2021.16.349)
12. Trusov P.V., Zaitseva N.V., Tsinker M.Yu., Babuskina A.V. Modelling dusty air flow in the human respiratory tract. *Russian Journal of Biomechanics*. 2018. V. 22. No. 3. P. 301–314 (in Russ.). doi: [10.15593/RZhBiomech/2018.3.03](https://doi.org/10.15593/RZhBiomech/2018.3.03)
13. Trusov P.V., Zaitseva N.V., Tsinker M.Yu. On modeling of airflow in human lungs: constitutive relations to describe deformation of porous medium. *PNRPU Mechanics Bulletin*. 2020. V. 4. P. 165–174 (in Russ.). doi: [10.15593/perm.mech/2020.4.14](https://doi.org/10.15593/perm.mech/2020.4.14)
14. Ertbruggen C.V., Hirsch C., Paiva M. Anatomically based three-dimensional model of airways to simulate flow and particle transport using computational fluid dynamics. *Journal of Applied Physiology*. 2004. V. 98. P. 970–980. doi: [10.1152/jappphysiol.00795.2004](https://doi.org/10.1152/jappphysiol.00795.2004)
15. Zhang Z., Kleinstreuer C., Donohue J.F., Kim C.S. Comparison of micro- and nano-size particle depositions in a human upper airway model. *Journal of Aerosol Science*. 2005. V. 36. № 2. P. 211–233. doi: [10.1016/j.jaerosci.2004.08.006](https://doi.org/10.1016/j.jaerosci.2004.08.006)
16. Huang J., Zhang L. Numerical simulation of micro-particle deposition in a realistic human upper respiratory tract model during transient breathing cycle. *Particuology*. 2011. V. 9. № 4. P. 424–431. doi: [10.1016/j.partic.2011.02.004](https://doi.org/10.1016/j.partic.2011.02.004)
17. Ou C., Hang J., Deng Q. Particle Deposition in Human Lung Airways: Effects of Airflow, Particle Size, and Mechanisms. *Aerosol and Air Quality Research*. 2020. V. 20. P. 2846–2858. doi: [10.4209/aaqr.2020.02.0067](https://doi.org/10.4209/aaqr.2020.02.0067)
18. Rahman Md.M., Zhao M., Islam M. S., Dong K., Saha S.C. Nanoparticle transport and deposition in a heterogeneous human lung airway tree: An efficient one path model for CFD simulations. *European Journal of Pharmaceutical Sciences*. 2022. V. 177. P. 106279. doi: [10.1016/j.ejps.2022.106279](https://doi.org/10.1016/j.ejps.2022.106279)

19. Choi J. *Multiscale numerical analysis of airflow in CT-based subject specific breathing human lungs*: PhD Dissertation. Iowa: University of Iowa, 2011. 259 p.
20. Wall W.A., Rabczuk T. Fluid structure interaction in lower airways of CT-based lung geometries. *Int. J. Num. Methods in fluids*. 2008. № 57. P. 653–675.
21. Lambert A.R., O’Shaughnessy P., Tawhai M.H., Hoffman E.A., Lin C.-L. Regional deposition of particles in an image-based airway model: large-eddy simulation and left-right lung ventilation asymmetry. *Aerosol Sci. Technol.* 2011. V. 45. № 1. P. 11–25. doi: [10.1080/02786826.2010.517578](https://doi.org/10.1080/02786826.2010.517578)
22. Rahman M., Zhao M., Islam M. S., Dong K., Saha S.C. Numerical study of nano and micro pollutant particle transport and deposition in realistic human lung airways. *Powder Technology*. 2022. V. 402. P. 117364. doi: [10.1016/j.powtec.2022.117364](https://doi.org/10.1016/j.powtec.2022.117364)
23. Katz I., Pichelin M., Montesantos S., Murdock A., Fromont S., Venegas J., Caillibotte G. The influence of lung volume during imaging on CFD within realistic airway models. *Aerosol Science and Technology*. 2017. V. 51. № 2. P. 214–223. doi: [10.1080/02786826.2016.1254721](https://doi.org/10.1080/02786826.2016.1254721)
24. Rahimi-Gorji M., Pourmehran O., Gorji-Bandpy M., Gorji T.B. CFD simulation of airflow behavior and particle transport and deposition in different breathing conditions through the realistic model of human airways. *Journal of Molecular Liquids*. 2015. V. 209. P. 121–133. doi: [10.1016/j.molliq.2015.05.031](https://doi.org/10.1016/j.molliq.2015.05.031)
25. Lin J., Fan J.R., Zheng Y.Q., Hu G.L., Pan D. Numerical simulation of inhaled aerosol particle deposition within 3D realistic human upper respiratory tract. *AIP Conference Proceedings*. 2010. V. 1207. № 1. P. 992–997. doi: [10.1063/1.3366500](https://doi.org/10.1063/1.3366500)
26. Naseri A., Shaghaghian S., Abouali O., Ahmadi G. Numerical investigation of transient transport and deposition of microparticles under unsteady inspiratory flow in human upper airways. *Respir. Physiol. Neurobiol.* 2017. V. 244. P. 56–72. doi: [10.1016/j.resp.2017.06.005](https://doi.org/10.1016/j.resp.2017.06.005)
27. Kiasadegh M., Emdad H., Ahmadi G., Abouali O. Transient numerical simulation of airflow and fibrous particles in a human upper airway model. *Journal of Aerosol Science*. 2019. V. 140. P. 105480. doi: [10.1016/j.jaerosci.2019.105480](https://doi.org/10.1016/j.jaerosci.2019.105480)
28. Qi S., Zhang B., Teng Y., Li J., Yue Y., Kang Y., Qian, W. Transient dynamics simulation of airflow in a CT-scanned human airway tree: More or fewer terminal bronchi? *Comput. Math. Methods Med.* 2017. V. 2017. P. 1969023. doi: [10.1155/2017/1969023](https://doi.org/10.1155/2017/1969023)
29. Weibel E.R. *Morfometriia legkikh cheloveka*. Moscow: 1970. 176 p. (Translation of: Weibel E.R. Morphometry of the Human Lung. Springer Verlag, Berlin-Göttingen-Heidelberg; 1963).
30. Bradshaw K., Warfield-McAlpine P., Vahaji S., Emmerling J., Salati H., Sacks R., Fletcher D.F., Singh N., Inthavong K. New insights into the breathing physiology from transient respiratory nasal simulation. *Physics of Fluids*. 2022. V. 34. № 11. P. 115103. doi: [10.1063/5.0112223](https://doi.org/10.1063/5.0112223)
31. Luo H.Y., Liu Y. Modeling the bifurcating flow in a CT-scanned human lung airway. *Journal of Biomechanics*. 2008. V. 41. № 12. P. 2681–2688. doi: [10.1016/j.jbiomech.2008.06.018](https://doi.org/10.1016/j.jbiomech.2008.06.018)
32. Qi S., Zhang B., Yue Y., Shen J., Teng Y., Qian W., Wu J. Airflow in Tracheobronchial Tree of Subjects with Tracheal Bronchus Simulated Using CT Image Based Models and CFD Method. *J. Med. Syst.* 2018. V. 42. № 4. P. 65. doi: [10.1007/s10916-017-0879-0](https://doi.org/10.1007/s10916-017-0879-0)
33. Rahimi-Gorji M., Gorji T.B., Gorji-Bandpy M. Details of regional particle deposition and airflow structures in a realistic model of human tracheobronchial airways: two-phase flow simulation. *Computers in Biology and Medicine*. 2016. V. 74. P. 1–17. doi: [10.1016/j.combiomed.2016.04.017](https://doi.org/10.1016/j.combiomed.2016.04.017)
34. Borziak E.I., Volkova L.I., Dobrovolskaia E.A., Revazov V.S., Sapin M.R. *Anatomiia cheloveka* (Human anatomy). Ed. M.R. Sapin. Moscow, 1993. Vol. 1. 544 p. (in Russ.).

35. Kukes V.G., Marinin V.F. *Clinical Diagnostic Methods (inspection, palpation, percussion, auscultation)*: Student's Manual. Moscow: GEOTAR-Media; 2006. 720 p. (in Russ.).
36. Zolotko Yu.L. *Topographic Atlas of Human Anatomy*. Moscow: Medicine; 1967. 272 p. (in Russ.).
37. Morgan G.E., Michael M.S. *Klinicheskaiia anesteziologiia*. M.-SPb.: BINOM-Nevskii Dialekt; 2001. 396 p. (Translation of: Morgan G.E., Michael M.S. *Clinical Anesthesiology*. v. 2. Appleton & Lange A Simon & Schuster Company; 1996. 747 p.).
38. *Fiziologiia dykhaniiia. Osnovy*. Moscow: Mir; 1988. 196 p. (Translation of: West J.B. *Respiratory Physiology - The Essentials*. Lippincott Williams and Wilkins, USA; 1985).
39. Giannaccini M.E., Yue K., Graveston J., Birchall M., Conn A., Rossiter J. Respiratory simulator for robotic respiratory tract treatments in Proc. *IEEE Int. Conf. Robot. Biomimet. (ROBIO)*. 2017. P. 2314–2319. doi: [10.1109/ROBIO.2017.8324764](https://doi.org/10.1109/ROBIO.2017.8324764)
40. Wilcox D.C. Reassessment of the Scale-Determining Equation for Advanced Turbulence Models. *AIAA Journal*. 1988. V. 26. № 11. P. 1299–1309. doi: [10.2514/3.10041](https://doi.org/10.2514/3.10041)
41. Schiller L., Naumann A. Über die grundlegenden Berechnungen bei der Schwerkraft aufbereitung. *Z. Verein Deutsch. Ing.* 1933. V. 77. P. 318–320.
42. Kostyuk I.F., Kapustnik V.A., Brykallin V.P., Kalmykov A.A. *Professional'nye bolezni: uchebnoe posobie* (Occupational diseases: a textbook). Ukraine, Kharkov, Kharkiv State Medical University, 2007. 155 p. (in Russ.).
43. Artemova, L.V., Baskova, N.V., Burmistrova, T.B., Buryakina, E.A. et al. *Federal'nye klinicheskie rekomendacii po diagnostike, lecheniyu i profilaktike pnevmokoniozov* (Federal Clinical Practice Guidelines for the diagnostics, prevention and treatment of pneumoconiosis). Ed. Izmerov N.F. Russia, Moscow, 2014. https://www.researchgate.net/publication/308414040_FEDERAL_CLINICAL_PRACTICE_GUIDELINES_FOR_THE_DIAGNOSIS_PREVENTION_AND_TREATMENT_OF_PNEUMOCONIOSIS (accessed 23.03.2026).
44. Artemova L.V., Baskova N.V., Burmistrova T.B., Buryakina E.A., Buhtiyarov I.V., Bushmanov A.Yu., Vasilyeva O.S., Vlasov V.G., Gorblyansky Y.Y., Zhabina S.A., Zaharinskaya O.N., Ismerov N.F., Kovalevsky E.V., Kuznetsova G.V., Kuzmina L.P., Kunyaeva T.A., Logvinenko I.I., Lutsenko L.A., Mazitova N.N., Obukhova T.Yu., Odintseva O.V., Orlova G.P., Panacheva L.A., Piktushanskaya I.N., Plyukhin A.E., Poteryaeva E.L., Pravilo S.V., Razumov V.V., Roslaya N.A., Roslyi O.F., Rushkevich O.P., Semenihi V.A., Serebryakov P.V., Smirnova E.L., Sorkina N.S., Tsidil'kovskaya E.S., Chasovskikh E.V., Shpagina L.A. Federal clinical recommendations on diagnosis, treatment and prevention of pneumoconiosis. *Russian Journal of Occupational Health and Industrial Ecology*. 2016. V. 1. P. 36–49 (in Russ.).

Received 20.02.2026.

Published 09.04.2026.